Terahertz bandwidth RF spectrum analysis of femtosecond pulses using a chalcogenide chip

M. D. Pelusi[1,*], T. D. Vo[1], F. Luan[1], S. J. Madden[2], D.-Y. Choi[2], D. A. P. Bulla[2], B. Luther-Davies[2], B. J. Eggleton[1]

[1] *ARC Centre for Ultrahigh bandwidth Devices for Optical Systems (CUDOS), Institute of Photonics and Optical Science (IPOS), School of Physics, University of Sydney, New South Wales 2006, Australia*
[2] *ARC Centre for Ultrahigh bandwidth Devices for Optical Systems (CUDOS), Laser Physics Centre, Australian National University, Canberra ACT 0200, Australia*
**m.pelusi@physics.usyd.edu.au*

Abstract: We report the first demonstration of the use of an RF spectrum analyser with multi-terahertz bandwidth to measure the properties of femtosecond optical pulses. A low distortion and broad measurement bandwidth of 2.78 THz (nearly two orders of magnitude greater than conventional opto-electronic analyzers) was achieved by using a 6 cm long As_2S_3 chalcogenide waveguide designed for high Kerr nonlinearity and near zero dispersion. Measurements of pulses as short as 260 fs produced from a soliton-effect compressor reveal features not evident from the pulse's optical spectrum. We also applied an inverse Fourier transform numerically to the captured data to re-construct a time-domain waveform that resembled pulse measurement obtained from intensity autocorrelation.

OCIS codes: (070.4340) Nonlinear optical signal processing; (070.4790) Spectrum analysis (190.4360) Nonlinear optics, devices; (190.7110) Ultrafast nonlinear optics.

References and links

1. J. P. Curtis, and J. E. Carroll, "Autocorrelation systems for the measurement of picosecond pulses from injection lasers," Int. J. Electron. **60**(1), 87–111 (1986).
2. R. Trebino, K. W. DeLong, D. N. Fittinghoff, J. N. Sweetser, M. A. Krumbügel, B. A. Richman, and D. J. Kane, "Measuring ultrashort laser pulses in the time-frequency domain using frequency-resolved optical gating," Rev. Sci. Instrum. **68**(9), 3277–3295 (1997).
3. J. Li, M. Westlund, H. Sunnerud, B.-E. Olsson, M. Karlsson, and P. A. Andrekson, "0.5-Tb/s eye-diagram measurement by optical sampling using XPM-induced wavelength shifting in highly nonlinear fiber," IEEE Photon. Technol. Lett. **16**(2), 566–568 (2004).
4. M. T. Kauffman, W. C. Banyai, A. A. Godil, and D. M. Bloom, "Time-to-frequency converter for measuring picosecond optical pulses," Appl. Phys. Lett. **64**(3), 270–272 (1994).
5. M. A. Foster, R. Salem, D. F. Geraghty, A. C. Turner-Foster, M. Lipson, and A. L. Gaeta, "Silicon-chip-based ultrafast optical oscilloscope," Nature **456**(7218), 81–84 (2008).
6. C. Dorrer, and D. N. Maywar, "RF Spectrum analysis of optical signals using nonlinear optics," J. Lightwave Technol. **22**(1), 266–274 (2004).
7. J. L. Blows, P. Hu, and B. J. Eggleton, "Differential group delay monitoring using an all-optical signal spectrum-analyser," Opt. Commun. **260**(1), 288–291 (2006).
8. T. Luo, C. Yu, Z. Pan, Y. Wang, J. E. McGeehan, M. Adler, and A. E. Willner, "All-optical chromatic dispersion monitoring of a 40-Gb/s RZ signal by measuring the XPM-generated optical tone power in a highly nonlinear fiber," IEEE Photon. Technol. Lett. **18**(2), 430–432 (2006).
9. G. P. Agrawal, *Nonlinear Fiber Optics* (Academic Press, San Diego, California, 3rd edition, 2001).
10. M. Pelusi, F. Luan, T. D. Vo, M. R. E. Lamont, S. J. Madden, D. A. Bulla, D.-Y. Choi, B. Luther-Davies, and B. J. Eggleton, "Photonic-chip-based radio-frequency spectrum analyser with terahertz bandwidth," Nat. Photonics **3**(3), 139–143 (2009).
11. M. Takahashi, R. Sugizaki, J. Hiroishi, M. Tadakuma, Y. Taniguchi, and T. Yagi, "Low-loss and low-dispersion-slope highly nonlinear fibers," J. Lightwave Technol. **23**(11), 3615–3624 (2005).
12. E. Tangdiongga, Y. Liu, H. de Waardt, G. D. Khoe, A. M. J. Koonen, H. J. S. Dorren, X. Shu, and I. Bennion, "All-optical demultiplexing of 640 to 40 Gbits/s using filtered chirp of a semiconductor optical amplifier," Opt. Lett. **32**(7), 835–837 (2007).
13. R. Salem, M. A. Foster, A. C. Turner, D. F. Geraghty, M. Lipson, and A. L. Gaeta, "Signal regeneration using low-power four-wave mixing on silicon chip," Nat. Photonics **2**(1), 35–38 (2007).
14. L. W. Couch II, *Digital and Analog Communication Systems* (Prentice Hall Inc. New Jersey, 1997).

#108701 - $15.00 USD Received 12 Mar 2009; revised 29 Apr 2009; accepted 5 May 2009; published 19 May 2009

15. S. J. Madden, D.-Y. Choi, D. A. Bulla, A. V. Rode, B. Luther-Davies, V. G. Ta'eed, M. D. Pelusi, and B. J. Eggleton, "Long, low loss etched As_2S_3 chalcogenide waveguides for all-optical signal regeneration," Opt. Express **15**(22), 14414–14421 (2007), http://www.opticsinfobase.org/oe/abstract.cfm?URI=oe-15-22-14414.
16. M. R. Lamont, C. M. de Sterke, and B. J. Eggleton, "Dispersion engineering of highly nonlinear As_2S_3 waveguides for parametric gain and wavelength conversion," Opt. Express **15**(15), 9458–9463 (2007), http://www.opticsinfobase.org/oe/abstract.cfm?URI=oe-15-15-9458.
17. S. V. Chernikov, E. M. Dianov, D. J. Richardson, and D. N. Payne, "Soliton pulse compression in dispersion-decreasing fiber," Opt. Lett. **18**(7), 476–478 (1993).
18. M. Scaffardi, F. Fresi, G. Meloni, A. Bogoni, L. Potí, N. Calabretta, and M. Guglielmucci, "Ultra-fast 160:10 Gbit/s time demultiplexing by four wave mixing in 1 m-long Bi_2O_3-based fiber," Opt. Commun. **268**(1), 38–41 (2006).
19. V. G. Ta'eed, L. Fu, M. Pelusi, M. Rochette, I. C. Littler, D. J. Moss, and B. J. Eggleton, "Error free all optical wavelength conversion in highly nonlinear As-Se chalcogenide glass fiber," Opt. Express **14**(22), 10371–10376 (2006), http://www.opticsinfobase.org/oe/abstract.cfm?URI=oe-14-22-10371.
20. T. Shoji, T. Tsuchizawa, T. Watanabe, K. Yamada, and H. Morita, "Low loss mode size converter from 0.3 μm square Si wire waveguides to singlemode fibres," Electron. Lett. **38**(25), 1669–1670 (2002).
21. M. D. Pelusi, F. Luan, E. Magi, M. R. Lamont, D. J. Moss, B. J. Eggleton, J. S. Sanghera, L. B. Shaw, and I. D. Aggarwal, "High bit rate all-optical signal processing in a fiber photonic wire," Opt. Express **16**(15), 11506–11512 (2008), http://www.opticsinfobase.org/oe/abstract.cfm?URI=oe-16-15-11506.
22. A. Prasad, C.-J. Zha, R.-P. Wang, A. Smith, S. Madden, and B. Luther-Davies, "Properties of $Ge_xAs_ySe_{1-x-y}$ glasses for all-optical signal processing," Opt. Express **16**(4), 2804–2815 (2008), http://www.opticsinfobase.org/oe/abstract.cfm?URI=oe-16-4-2804.

1. Introduction

Progress in high-speed optical communications, and applications of ultra-fast phenomena, demand advanced diagnostic tools that can monitor short pulses of broad spectral width. This is generally achieved using ultra-fast nonlinear optics, most commonly for temporal waveform measurement by the various techniques of intensity autocorrelation [1], FROG [2] or optical sampling [3]. High resolution measurements of short pulses can also be performed by a time lens scheme [4], which has recently demonstrated the performance advantage of using nonlinear optics in more compact, chip-based devices [5]. Beyond temporal measurements, another useful diagnostic is the radio-frequency (RF) spectrum of a pulse, given by the power spectrum of its temporal intensity waveform. This is routinely used in telecommunications and microwave photonics for characterizing distortions in amplitude or phase, and it is typically measured using an electrical spectrum analyzer with an expensive high-speed photo-detector. The measurement bandwidth of this system is, however, limited by the electronics to several tens of gigahertz, which is inadequate for emerging higher bandwidth applications.

An alternative approach for RF spectrum measurement has been demonstrated using ultrafast nonlinear effects during propagation of the signal with a cw probe in hundreds of meter lengths of silica-based highly nonlinear fiber (HNF). This scheme, shown schematically in Fig. 1(a), enables the signal RF spectrum to be captured on an optical spectrum analyzer (OSA) with measurement bandwidths of ≈800 GHz [6]. Its effectiveness for performance monitoring of 40 Gb/s signals [7], [8] has been demonstrated. However, capturing the broader RF spectrum of shorter pulses, also relies on avoiding chromatic dispersion in the waveguide, which can distort the signal under test, and weaken its nonlinear interaction with the co-propagating probe due to their group-velocity mismatch [9], i.e. "walk-off".

To remedy this, we recently reported a photonic-chip based RF spectrum analyzer (PC-RFSA) [10], employing a dispersion-shifted chalcogenide (ChG) waveguide with a nonlinearity coefficient (γ) of several hundreds times larger than silica-based HNF [11]. This allowed use of a shorter (centimeter scale), and low dispersion waveguide to enhance the measurement bandwidth and reduce signal distortion. In contrast to other nonlinear chip-scale devices such as semiconductor optical amplifiers [12], and silicon waveguides [5], [13], ChG avoids free-carrier effects which can complicate pulse propagation dynamics. Our PC-RFSA used a 16 cm long waveguide, to demonstrate a multi-terahertz measurement bandwidth (for a 20 nm wavelength signal-probe separation) and the measurement of 320 Gb/s signals [10].

In this paper we take advantage of the broadband and low distortion capability of the PC-RFSA to achieve multi-THz span RF spectrum analysis of much shorter, sub-picosecond

#108701 - $15.00 USD Received 12 Mar 2009; revised 29 Apr 2009; accepted 5 May 2009; published 19 May 2009

pulses. This demands a much broader wavelength separation between the signal and probe, to accommodate the broader pulse spectrum under test. To counter the corresponding increase in walk-off, we used a shorter 6 cm long dispersion-shifted As_2S_3 waveguide, with higher γ. This led to a broader measurement bandwidth of 2.78 THz for a signal-probe wavelength separation of 50 nm. The PC-RFSA was used to measure pulses as short as 260 fs produced from a soliton-effect compressor, and revealed features such as temporal width and amplitude distortions (associated with non-optimum compression), that are not easily inferred from its optical spectrum. We also investigated numerical processing of the captured traces by an inverse Fourier transform, to reconstruct a time-domain waveform that resembled the pulses measured by autocorrelation [1]. This emphasizes the broadband capability of the PC-RFSA for capturing the RF spectrum of such short pulses spanning multi-terahertz bandwidths.

2. Operating principle and waveguide properties

Figure 1(a) shows the schematic of the all-optical RF spectrum analyzer [6]. Measuring the RF spectrum of an optical signal requires capturing the power spectrum of its intensity waveform (I) according to $G(f) = |\mathfrak{F}[\ I(t)]\ |^2$, where $\mathfrak{F}$ denotes the Fourier transform [9], [14] from time (t) to frequency (f) domains according to $\mathfrak{F}[I(t)] = \int I(t)\cdot exp(j\cdot 2\pi f\cdot t)dt$, where the integration is over t from $-\infty$ to $+\infty$. This function is distinct from the power spectrum of the signal electric field (E), given by $S(f) = |\mathfrak{F}[E(t)]|^2$, which is measured directly by an OSA. Figure 1(b) compares the calculated $G(f)$ and $S(f)$ for a hypersecant function $\{I(t) = sech^2(t)\}$ broadened by different amounts of dispersion. The curves highlight how $G(f)$ narrows inversely with pulse width while $S(f)$ remains unchanged, which is the well known basis for dispersion monitoring [7], [8], [10].

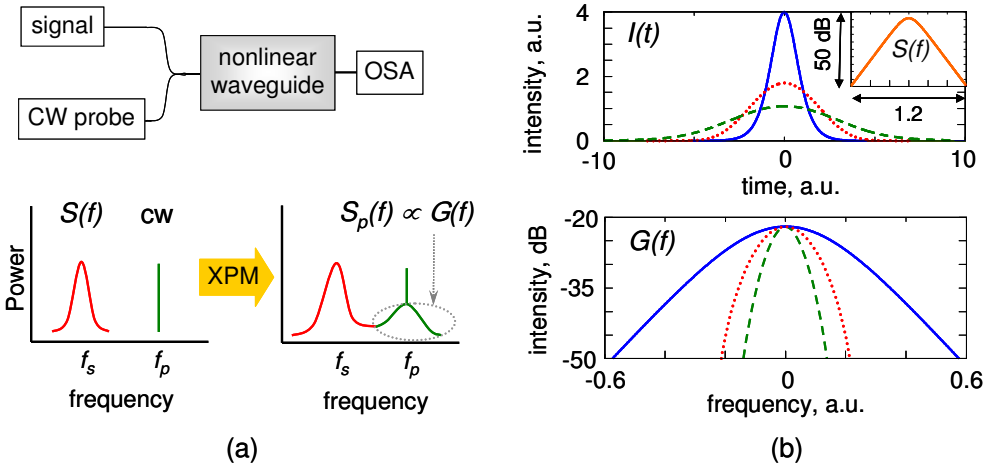

Fig. 1. (a). Schematic principle of the all-optical RF spectrum analyzer, making use of XPM in a nonlinear waveguide to capture the power spectrum of a signal's intensity given by $G(f) = |\mathfrak{F}[I(t)]|^2$, which is distinct from optical spectrum of the signal itself given by $S(f) = |\mathfrak{F}[E(t)]|^2$. (b) Comparison of calculated (top) temporal waveforms, $I(t)$, (inset) optical spectra, $S(f)$ and (lower) RF spectra, $G(f)$ for a hypersecant shape pulse, that is either (solid curve) Fourier transform-limited, or dispersed by linear propagation over a distance of (dotted curve) 2 L_d, or (dashed curve) 5 L_d, where L_d is the pulse dispersion-length [9].

Measuring $G(f)$ without the bandwidth constraints of a photo-detector connected to an electrical spectrum analyser, was demonstrated using the optical Kerr-effect of a waveguide during co-propagation of the signal at center frequency f_s, with a weaker cw probe at frequency f_p [6]. By this all-optical approach, the waveguide refractive index (n) varies temporally with $I(t)$ according to $n(I) = n_0 + n_2\cdot I$, where n_0 and n_2 are the linear and nonlinear

#108701 - $15.00 USD Received 12 Mar 2009; revised 29 Apr 2009; accepted 5 May 2009; published 19 May 2009

refractive indices respectively. For an optical signal power, P (related to intensity by $I = P/A_{eff}$ where A_{eff} is the effective mode area [9]), the probe undergoes cross-phase modulation (XPM) in proportion to $\Delta\phi = P \cdot \gamma \cdot L$ (ignoring propagation losses) [9], where L is the waveguide length, and γ the nonlinearity coefficient given by $\gamma = (2\pi/\lambda_s)\bullet(n_2/A_{eff})$ for a signal wavelength λ_s corresponding to f_s. This generates frequency modulation sidebands around the monochromatic probe whose output electric field (of normalized amplitude) at f_p is given by $E_p = exp(-j2\pi f_p t) \cdot exp(jk\Delta\phi)$ where k is a constant. For $\Delta\phi \ll 1$ (such that the exponential series is $exp(jk\Delta\phi) \approx \{1 + jk\Delta\phi\}$), its output optical spectrum becomes $S_p(f) \propto |\gamma L|^2 \bullet G(f-f_p)$, which enables $G(f)$ to be measured on an OSA [6]. The ultra-fast response of the Kerr-effect, originating from the $\chi^{(3)}$ susceptibility of the waveguide material [9] allows this to be performed with an enormous measurement bandwidth spanning 10 THz in principle.

In practice however, the measurement bandwidth is limited by the waveguide dispersion parameter, D, which can both distort the signal under test and weaken the XPM efficiency due to walk-off between the co-propagating signal and probe [10]. The scaling of efficiency with wavelength separation, therefore poses a challenge for measuring broader pulse spectra. The PC-RFSA on the other hand, takes advantage of As_2S_3 glass's high $n_2 \approx 3 \times 10^{-18}$ m^2/W (≈100 times of silica) and the ability to tailor A_{eff} to small dimensions. This allows D to be shifted closer to zero at 1550 nm, and produce higher γ in shorter waveguides, thereby providing the performance advantages of a distortion-free broad measurement bandwidth.

Chip fabrication [15] involved depositing a 0.85 μm thick film of As_2S_3 ($n_0 \approx 2.4$) on an oxidized silicon wafer ($n_0 = 1.44$) by thermal evaporation. From this, 6 cm long straight ribs, 2 μm wide, were formed by photolithography and dry-etching. The chip was then over-clad with a polymer layer ($n_0 = 1.51$) [15], hand-cleaved and coupled to lensed fibers with a 2.5 μm spot diameter giving a total insertion loss of ≈14.4 dB (between its fiber connectors) for the fundamental transverse magnetic (TM) mode. This was constituted by coupling and propagation losses of approximately 10.5 dB and 0.65 dB/cm, respectively. Mode solving by the Finite Element Method predicted the fundamental TM mode with $A_{eff} \approx 1.2$ μm^2 at 1550 nm corresponding to $\gamma \approx 9900$ W^{-1}km^{-1} at 1550 nm. This is notably higher than for our previous waveguide [10], which helps compensate for its shorter length. The schematic of the 6 cm size chip is shown in Fig. 2(a).

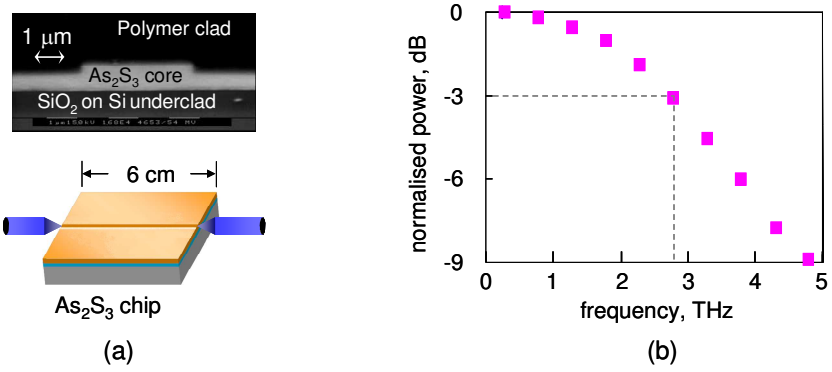

Fig. 2. (a). (Upper) Micrograph image of typical As_2S_3 planar rib waveguide cross-section, and (lower) schematic of the 6 cm size chip coupled to lenzed fibers. (b) The measurement bandwidth of the PC-RFSA determined from the power of the side-band tone generated around the probe by XPM, as a function of the input signal sine-wave frequency, when signal and probe are separated by 50 nm.

As with our original PC-RFSA [10], fabrication of such a small-dimension rib waveguide induces significant waveguiding dispersion with an opposite sign to the large (and normal) material dispersion of As_2S_3 glass (–357 ps/nm.km at 1550 nm wavelength [15]). This enabled D to be tuned to small or even anomalous values [16]. Mode solving shows this is achieved when the field penetrates the top of the rib, and indicated that D was shifted to ≈28

#108701 - $15.00 USD Received 12 Mar 2009; revised 29 Apr 2009; accepted 5 May 2009; published 19 May 2009

ps/nm.km (i.e. anomalous). To take advantage of this, both signal and probe were coupled to the TM mode using fiber polarization controllers (PC's) positioned before the waveguide. This simultaneously ensured their polarization states were aligned for maximum XPM.

3. Experimental results

An advantage of using a short, low dispersion waveguide in the PC-RFSA is the broadened measurement bandwidth. This was experimentally characterized using a sinewave optical signal formed by the interference of two, equal power, cw lasers with tunable wavelength separation centred at λ_s = 1550 nm [6]. The polarization states of both lasers were aligned by PC's to maximize the sinewave modulation depth. The beat signal was then combined with a cw probe at wavelength, λ_p = 1600 nm, and launched into the waveguide with total average powers at its input connector being 48 mW, and 32 mW respectively. The power of the XPM tone generated around λ_p was then measured while tuning the sinewave beat frequency to obtain the curve in Fig. 2(b). This indicated that the 3 dB single-sided bandwidth was 2.78 THz, which covers the frequency range of interest for the pulses generated from our source. It is important to note, that this measurement used a 2.5 times wider signal-probe wavelength separation than our original PC-RFSA [10], which highlights its performance advantage in terms of walk-off, as described in more detail in Section 4. In other words, a narrower bandwidth would be expected if the longer 16 cm waveguides were used.

The impact of the waveguide's dispersion on short pulse propagation was investigated from autocorrelation measurements. The source shown in Fig. 3(a) was used to generate pulses with ≈11 nm spectral width (estimated from the OSA trace in Fig. 3(b)), which equates to a Fourier transform-limited pulse width of ≈230 fs. These were launched into the waveguide at an average power of 16 mW at the input connector. The output was then measured on an intensity autocorrelator (of second-harmonic generation (SHG) type [1]) via an erbium-doped fiber amplifier (EDFA). This revealed high quality pulses with full width at half maximum (FWHM) duration of 260 fs, as shown in Fig. 3(b). The measurement was then repeated with the waveguide substituted by a variable optical attenuator (VOA) of comparable length (from connector to connector), and its attenuation matched to the waveguide insertion loss. This produced nearly identical output pulses of 250 fs FWHM as shown, highlighting the low distortion achieved, as expected from the dispersion length calculations described in Section 4.

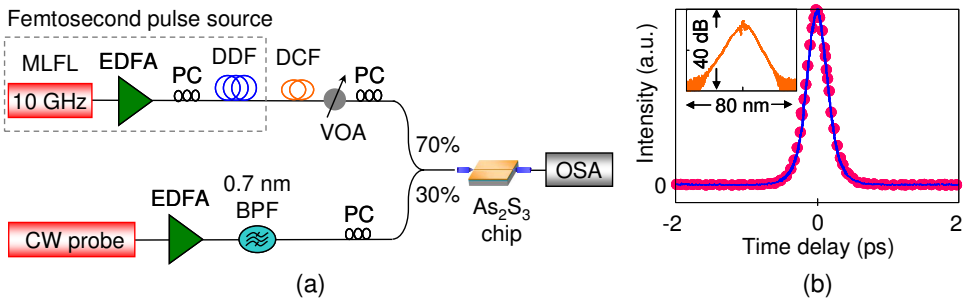

Fig. 3. (a). Experimental setup of the PC-RFSA for measuring the RF spectrum of femtosecond pulses generated from a DDF (b) Evaluation of pulse broadening in the As_2S_3 chip by measuring the intensity autocorrelation of the optical field reaching the OSA, either with the (blue solid curve) chip in place, or (red dots) substituted for a VOA. The pulse FWHM are 260 and 250 fs respectively. (Inset) Optical spectrum of DDF output measured on an OSA.

The RF spectrum measurement was then performed using the PC-RFSA set-up shown in Fig. 3(a). The pulse source consisted of an active mode-locked fiber laser (MLFL) emitting ~2 ps pulses at 10 GHz repetition rate and 1540 nm center wavelength. These were boosted in an EDFA and launched into a dispersion-decreasing fiber (DDF), with energy corresponding to approximately a fundamental soliton. The DDF was designed with a dispersion parameter continuously decreasing along its 340 m length, to induce adiabatic soliton compression [17].

#108701 - $15.00 USD Received 12 Mar 2009; revised 29 Apr 2009; accepted 5 May 2009; published 19 May 2009

For an optimum average launch power of 126 mW (i.e. 6 W peak power and 13 pJ energy), the DDF emitted high quality fundamental soliton pulses of 260 fs FWHM, as shown from the intensity autocorrelation measurement in Fig. 4a(i). Although the temporal waveform closely fitted a sech^2 pulse shape, the optical spectrum measured on an OSA appeared distorted, as shown in Fig. 4a(ii). This is indicative of non-ideal compression associated with too rapid a perturbation of the soliton energy along the DDF (with respect to the pulse dispersion length, L_d [9]). The result is the formation of a broad lower intensity pedestal in the time domain that spectrally interferes with the soliton. This complicates reading the pulse bandwidth from its conventional FWHM, which in turn complicates inference of the Fourier transform-limited pulse width from the expected time-bandwidth product of 0.315 for a hypersecant pulse. At a higher input power to the DDF of 251 mW, the pulse spectrum was further broadened and distorted, as shown in Fig. 4b(ii). Intensity autocorrelation measurements also indicated temporal broadening to 390 fs (Fig. 4b(i)).

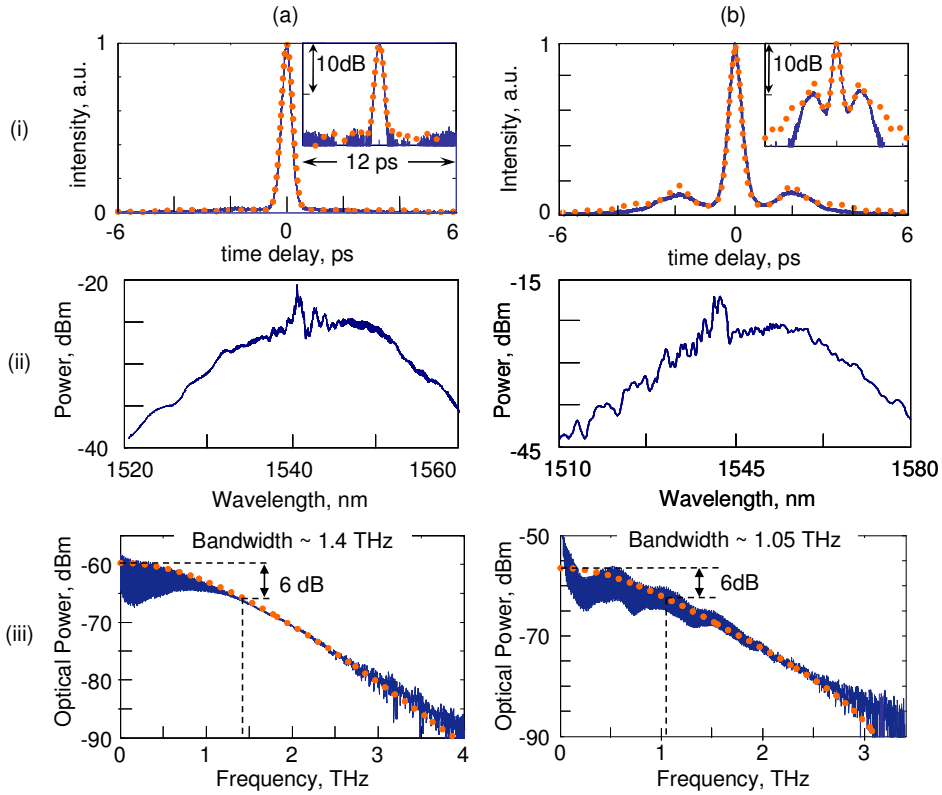

Fig. 4. Measurement traces of soliton-compressed pulses emitted from a DDF, for different input launch powers of (a) 126 mW, and (b) 251 mW, captured as (i) temporal waveforms from (solid curve) SHG intensity autocorrelator, and (dots) reconstruction by numerical processing of PC-RFSA output RF spectra, and plotted in linear and (inset) log scales, (ii) optical spectra from an OSA and (iii) (solid curve) RF spectra from the PC-RFSA, compared to (dotted curve) numerically calculated sech^4 fit.

The RF spectrum was then measured by launching the pulses at λ_s = 1540 nm into the PC-RFSA with a 32 mW cw probe at λ_p = 1600 nm. The total average launch power at the waveguide input connector was ≈100 mW. Such a wide wavelength separation between the signal and probe was essential to accommodate the very broad pulse bandwidths generated by the source without spectrally interfering with the XPM broadened probe. This emphasizes the advantage of using the short, dispersion-shifted ChG waveguide (as discussed in Section 4). A few meters of dispersion compensating fiber (DCF) was also inserted before the PC-RFSA to

#108701 - $15.00 USD Received 12 Mar 2009; revised 29 Apr 2009; accepted 5 May 2009; published 19 May 2009

compensate for pulse dispersion during transmission in the standard single-mode fibers between the DDF output and PC-RFSA input.

The RF spectra of the soliton-compressed pulses corresponding to both optimum and higher DDF input power are shown in Fig. 4(iii). The measurement trace with ≈35 dB dynamic range represents a single side-band of the XPM broadened probe captured by the OSA, using a spectral resolution of 0.01 nm (≈1.2 GHz) with the wavelength axis converted to frequency. Unlike for the optical spectra in Fig. 4(ii), the envelopes of the RF spectra more closely follow hypersecant functions. The rippling in the RF spectrum envelope observed for higher input power to the DDF is associated with the temporal waveform distortion corresponding to the pedestal wings in the autocorrelation trace of Fig. 4b(i).

To test how truly representative the RF spectrum measurement is of the pulse, we investigated the numerical processing of the data to reconstruct a temporal waveform that could be compared to SHG autocorrelation measurements. This was performed by numerically deleting the probe component, and taking half of the remaining power spectrum ($X(f)$) i.e. the longer wavelength sideband, and combining it with a mirror image of itself (in frequency) to form $G(f)$. The operation described in Sect. 2 was then reversed to reconstruct $I(t)$ by taking an inverse Fourier transform of $[G(f)]^{1/2}$. To compare this with measurements from a SHG type autocorrelator, the autocorrelation of $I(t)$ was generated by applying the operation $A(\tau) = \int I(t)I(t-\tau)\,dt$ (where $\int$ denotes integration from $+\infty$ to $-\infty$). These displayed good agreement with the SHG measurement traces as shown in Fig. 4(i). Their FWHM for both the optimum and higher input power into the DDF were 300 fs and 380 fs respectively.

The autocorrelation waveform has an important relation to $G(f)$ by the Wiener-Khintchine thereom [14] which states that the RF spectrum equals the Fourier transform of the autocorrelation function, i.e. $G(f) = F(A(\tau))$. This allows the autocorrelation waveforms plotted in Fig. 4(i) to be reconstructed more directly by simply taking an inverse Fourier transform of $G(f)$.

While the Wiener-Khintchine theorem provides an exact, direct relation between the RF spectrum and autocorrelation, it is well known that the autocorrelation cannot always unambiguously retrieve the shape of more complex pulses [1], and there exists the possibility of different pulses possessing the same autocorrelation. Considering an asymmetric pulse shape for example, the temporal intensity would Fourier transform into a complex function, whose phase information would be lost in the power spectrum, leading to a symmetric autocorrelation. These limitations would equally apply to the reconstructed $I(t)$. Nevertheless, its ability to resolve temporal features such as pedestal is effectively shown.

The temporal resolution of the reconstructed waveform is determined by the sampling point time step which from discrete Fourier transform theory [14] equals $1/(N.df)$ where N and df are the number of samples and sampling frequency for $G(f)$ respectively. In our example, $X(f)$ contained 2960 samples with df corresponding to a wavelength step of 0.01 nm. Achieving a sampling time under 100 fs for the waveform trace required increasing N from 5920 to 12060 points by appending an expanded noise floor to $G(f)$ out to higher frequencies.

4. Discussion

The spectral bandwidth of a pulse provides a useful means to infer the temporal FWHM (T) of a known waveform via its time-bandwidth product. For a hypersecant pulse, this is given by $T \times F_{osa} = 0.315$, where F_{osa} is the spectral FWHM (in frequency) of $S(f)$ measured on an OSA. However, distortion of the optical spectrum as in Fig. 4(b) often makes estimation of F_{osa} unreliable. In such cases, the RF spectrum can be more effective. However, this requires a modified constant for the time-bandwidth product. This can be determined for a soliton by considering its intensity in normalized units given by $I(t) = sech^2(t)$, whereby $T = 1.763$. The corresponding optical spectrum can be shown to be $S(f) = sech^2(1.763^2 f/0.315)$ with $F_{osa} = 0.315/1.763$. The RF spectrum found by numerical fit is $G(f) = sech^4(4f)$. By noting that the 3 dB (FWHM) bandwidth of $[G(f)]^{1/2} = sech^2(4f)$ equaling 1.763/4 is equivalent to the 6 dB bandwidth of $G(f)$ denoted F_{rf}, we obtain the ratio of $F_{osa}/F_{rf} = 0.405$. So the modified time-

#108701 - $15.00 USD Received 12 Mar 2009; revised 29 Apr 2009; accepted 5 May 2009; published 19 May 2009

bandwidth product in terms of the 6 dB *single-sided* bandwidth of $G(f)$ denoted ΔF_{6dB} becomes $T \times \Delta F_{6dB} = 0.388$. This was applied to the RF spectrum traces in Fig. 4c using the ΔF_{6dB} readings of 1.41 THz and 1.05 THz for the optimized and higher input DDF power examples respectively. This translates to T of 275 fs and 370 fs respectively which are within 5% and 8% of the FWHM obtained from the measured autocorrelation and numerically processed RF spectra of Fig. 4(i) respectively.

The PC-RFSA's performance advantages, in terms of its broadened measurement bandwidth and improved accuracy, stem from the waveguide's broadband low dispersion, which minimizes both distortion of the signal, and group velocity mismatch with the probe [9]. For a wavelength separation between signal and probe of $\Delta\lambda$ = 50 nm, the walk-off length whereby the delay due to group-velocity mismatch equals half a period of the sinewave signal of frequency f_{max} can be estimated by the equation, $L_w = 1/|f_{max}\,\Delta\lambda\,(2D - S\Delta\lambda)|$, where S is the dispersion slope i.e. variation of D with wavelength. This implies that walk-off would be negligible for f_{max} « 6 THz (in order to satisfy L_w » 6 cm assuming S = 0), which is consistent with the measurement bandwidth from Fig. 2. Its inverse scaling with L as plotted in Fig. 5, means f_{max} reduces to « 2.2 THz for a 16 cm length waveguide, (as was used in our original PC-RFSA [10]), assuming the same $\Delta\lambda$ and D values. It also highlights how the walk-off effect diminishes sharply for L < 6 cm, and varies significantly for $\Delta\lambda$ values between 20 and 60 nm. Note, given $\Delta\lambda$ is so large, a more accurate calculation of f_{max} would account for non-zero S and higher-order dispersion terms.

In terms of measurement accuracy, the dispersion length L_d [9] whereby the width of a pulse of initial FWHM, T, broadens significantly is given by $L_d = 2\pi\, c{\cdot}T^2/\{3.11\,|D|\,(\lambda_s)^2\}$, where a hyper-secant pulse shape is assumed. This implies that pulse broadening would be negligible in the waveguide for T » 81 fs (in order to satisfy L_d » 6 cm), which is consistent with the negligible dispersion observed for the 250 fs pulse in Fig. 3(b). Scaling this to L = 16 cm with the same D value, gives T » 133 fs as shown in Fig. 5.

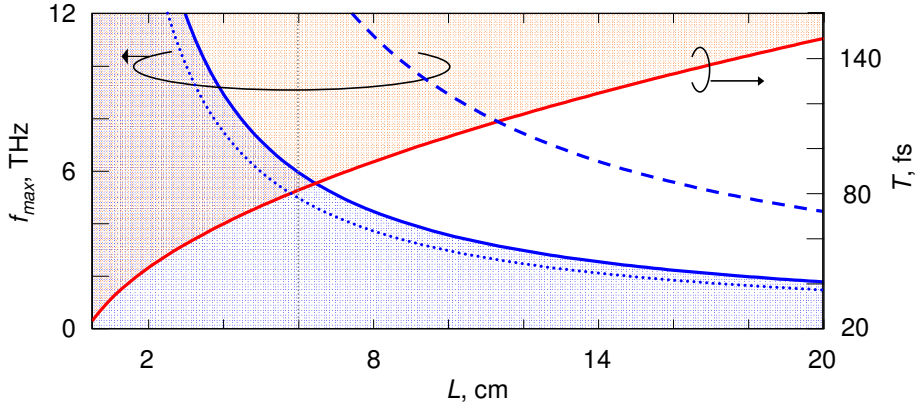

Fig. 5. Chromatic dispersion effect on the performance limits of the PC-RFSA, in terms of the approximate asymmtotic maximum measurement bandwidth (f_{max}) and minimum FWHM (T) of a hyper-secant pulse-shape for distortion-free transmission through a waveguide of length L, for (solid curves) $\Delta\lambda$ = 50 nm, (dashes) $\Delta\lambda$ = 20 nm, and (dots) $\Delta\lambda$ = 60 nm assuming D = 28 ps/nm.km, S = 0, and λ_s = 1550 nm.

These calculations were repeated using the parameters of various HNF assuming an equal $\gamma.L$ product as our chip of 0.59 W^{-1} for comparison. Considering a dispersion-flattened silica HNF (i.e. S = 0), with typical values of D = 0.5 ps/nm.km, and γ = 20 $W^{-1}km^{-1}$ at 1550 nm, the equivalent longer L of 29.7 m would translate to f_{max} « 673 GHz and T » 241 fs. Although alternate HNF based on either Bi_2O_3 [18], or ChG [19], have reported higher γ values of 1250 and 1200 $W^{-1}km^{-1}$ respectively, translating to equivalent shorter L of 47 and 50 cm respectively, both fibers also exhibit large normal dispersion parameters of D = −310 and −560 ps/nm.km at 1550 nm respectively. Consequently, their respective performance

#108701 - $15.00 USD Received 12 Mar 2009; revised 29 Apr 2009; accepted 5 May 2009; published 19 May 2009

parameters (assuming $S = 0$) are degraded to f_{max} « 68 GHz and 36 GHz, and T » 0.73 ps and 1.05 ps. These calculations highlight the potential performance advantage of dispersion-shifted and highly nonlinear chip-scale devices, particularly when considering very broadband pulses.

There are several routes to improving the performance of the PC-RFSA including lowering the insertion loss and increasing the nonlinear response. The large coupling loss, arising from the overlap mismatch between the modes of the lensed fiber and rib waveguide, could be significantly improved by incorporating on-chip tapers, as demonstrated for silicon waveguides [13]. Losses below 1 dB per facet for coupling from nano-scale rib waveguides into standard single mode fiber has been reported by various tapering techniques [20]. A lower propagation loss (of around half) is also expected from optimizing the rib etching process to reduce its surface roughness, which for lower rib heights (i.e. thinner ChG films), leads to an increased scattering loss as more of the mode field penetrates it. Both improvements would permit an insertion loss comparable to the 4.5 dB value demonstrated for a tapered As_2S_3 fiber of similar length and A_{eff} [21]. Finally, use of alternative chalcogenide glasses, such as $Ge_{11}As_{22}Se_{67}$ [22], would offer about a factor of four increased nonlinear response compared with As_2S_3. Such advances would permit a higher dynamic range for the measurement or operation with even lower optical launch powers.

5. Conclusions

Analysis of femtosecond pulses from their RF spectrum spanning multi-THz bandwidths has been demonstrated for the first time through the use of a 6 cm long dispersion-shifted chalcogenide waveguide. The combined high nonlinearity, and broadband low dispersion, enabled the RF spectrum of pulses as short as 260 fs to be measured with negligible pulse broadening within the waveguide, achieving a broad measurement bandwidth of 2.78 THz. Characterization of pulses from a soliton-effect compressor revealed temporal features that could not be observed by conventional optical spectrum measurements alone. Furthermore, numerical processing of the RF spectrum was investigated as a means for reconstructing the temporal waveform, which showed good agreement with pulses measured by intensity autocorrelation, in terms of pulse shape, width and pedestal. Also, the use of the Weiner-Khintchine theorem enabled the autocorrelation to be directly generated by an inverse Fourier transform of the RF spectrum. The results highlight the effectiveness of this scheme as a useful diagnostic tool for the characterization of ultra-short pulses.

Acknowledgments

The authors gratefully acknowledge Dr. A. Sysoliatin at the Fiber Optics Research Center at the General Physics Institute, Moscow, Russia for providing the DDF used in the soliton-effect pulse compressor. This work was supported in part by the Australian Research Council (ARC) through its ARC Centres of Excellence and Federation Fellowship programs.

#108701 - $15.00 USD Received 12 Mar 2009; revised 29 Apr 2009; accepted 5 May 2009; published 19 May 2009